ELSEVIER

Contents lists available at ScienceDirect

International Journal of Applied Earth Observation and Geoinformation

journal homepage: www.elsevier.com/locate/jag





Automatic mapping of aquaculture activity in the Atlantic Ocean

Xabier Lekunberri ^{a,b,*}, J. David Ballester-Berman ^c, Ignacio Arganda-Carreras ^{b,d,e,f}, Jose A. Fernandes-Salvador ^a

- a AZTI, Marine Research, Basque Research and Technology Alliance (BRTA), Txatxarramendi Ugartea z/g, Sukarrieta, Bizkaia 48395, Spain
- ^b University of the Basque Country (UPV/EHU), San Sebastian, Spain
- ^c Institute for Computer Research (IUII), University of Alicante, Spain
- ^d IKERBASQUE, Basque Foundation for Science, Bilbao, Spain
- ^e Donostia International Physics Center (DIPC), San Sebastian, Spain
- f Biofisika Institute (CSIC, UPV/EHU), Leioa, Spain

ARTICLE INFO

Keywords:
Environmental impacts
Remote sensing
Big data
Water quality
Sentinel-1
Aquaculture mapping

ABSTRACT

The production of wild fish has remained relatively stable in the last two decades, whereas aquaculture organism production has increased to the point where it has exceeded wild catches. In this context, accurate and up-to-date information about the current usage of marine areas for aquaculture is crucial for the planning of marine activities. However, this data is often limited to national authorities, and discrepancies between planned and real practices can arise in available data. In this study, a novel methodology to automatically map and verify the current activity of aquaculture crops across European regions based on freely available satellite data is proposed. The European Space Agency's (ESA) Sentinel-1 mission provides Synthetic Aperture Radar (SAR) images, which serve as the basis for the analysis. Multiple SAR images of the same locations are processed using ESA Sentinel Application Platform (SNAP) software and merged to remove temporal noise-like artifacts caused by factors such as ships and waves. Next, the iDPolRAD algorithm is employed to detect potential aquaculture sites, which initially include noise from coastal zones and unwanted human and natural structures that pass through the filter. The aquaculture sites are classified using a ResNet18 model with 93% of the sites correctly classified. This implies that it is feasible to monitor marine areas using satellite radar data to track aquaculture areas. However, generalization power across regions is poor likely due to the diversity of types of structures used and species cultivated. Further studies are needed to investigate factors influencing the detectability of different aquaculture sites such as cage geometry or SAR image resolution in order to enhance the accuracy and comprehensiveness of the mapping process. This study highlights the potential of SAR data, coupled with image processing and classification techniques, as a viable means to map large marine areas dedicated to aquaculture.

1. Introduction

Wild fish catches have remained stable over the past two decades and are projected to decline due to climate change (Erauskin-Extramiana et al., 2023; Lotze et al., 2019; Tittensor et al., 2021). In contrast, the production of aquatic organisms from aquaculture is increasing, surpassing wild catches, with global aquaculture production of fish for human consumption and aquatic plants reaching a record 114.5 million tons in 2018 (FAO, 2020). In the same year, aquaculture production in the European Union (EU) reached 3.4 million tons, with mollusks, particularly mussels (39 %), Atlantic salmon (Salmo salar, 13 %), and

Rainbow trout (Oncorhynchus mykiss, 13 %) dominating the production. While global mussel production is increasing, it has been declining in the EU for several decades (Avdelas et al., 2021). Spain leads EU production, accounting for 45 % of the total weight, followed by Italy, France, the Netherlands, Great Britain, and Ireland (Hough, 2022). Scotland is the top producer of diadromous fishes in the EU, particularly salmon (Maire et al., 2021).

Aquaculture operations can impact ecosystems in various ways, including disease transmission between farms and wildlife, water pollution, salinization, and soil acidification (Martinez-Porchas & Martinez-Cordova, 2012). These activities may also lead to conflicts

E-mail address: xlekunberri@azti.es (X. Lekunberri).

^{*} Corresponding author at: AZTI, Marine Research, Basque Research and Technology Alliance (BRTA), Txatxarramendi Ugartea z/g, Sukarrieta, Bizkaia 48395, Spain.

with existing fisheries and trade-offs with other ecosystem services (Alleway et al., 2019; Coccoli et al., 2018). Modern fisheries and marine spatial planning aim to follow an ecosystem-based approach that requires consideration of all human activities and their pressures including aquaculture (Dong et al., 2024; Fernandes et al., 2023; Pedreschi et al., 2019). The rapid growth of aquaculture and its regional management makes it difficult to track its presence at a large scale beyond the national level (Fernandes-Salvador et al., 2021). In addition, current available mapping from regional and national authorities might not distinguish between areas where exploitation is allowed or planned and areas where the activity is already present. Given the above, the development of new methodologies for the control of this type of activity may be necessary.

One way to solve this could be to have an alternative observationbased method to collect international data, and not rely on different authorities to get it. Earth observation data emerges as this alternative not dependent on the public reporting of each region. The availability of earth observation data has exponentially increased since 2014, when the first satellite of the Copernicus program was launched. The Copernicus Earth observation program (Regulation (EU) No 377/2014 of the European Parliament and of the Council of 3 April 2014 Establishing the Copernicus Programme and Repealing Regulation (EU) No 911/2010 Text with EEA Relevance, 2014) is implemented by the European Member States, the European Space Agency (ESA), the European Organization for the Exploitation of Meteorological Satellites (EUMET-SAT), the European Centre for Medium-Range Weather Forecasts (ECMWF), EU Agencies and Mercator Ocean, being aimed at monitoring the globe with high quality and freely accessible data. This program started in 1998 and is based on satellite and in situ observations (Borgeaud et al., 2015). Currently, it includes the Sentinel missions, which are made up of both dedicated satellites and instruments onboard EUMETSAT's weather satellites. These Sentinel missions consist of several satellites that provide different types of remote sensing data. The first of these missions, Sentinel-1 (Torres et al., 2012), was composed of two twin satellites (Sentinel-1A and Sentinel-1B, the latter having ended its mission at the beginning of August 2022 due to an unexpected failure in the radar antenna power supply unit) sharing the same polar orbit. They are equipped with a Synthetic Aperture Radar (SAR), so they can capture data day and night and under almost any weather condition (ESA Communications, 2012; Geudtner et al., 2021). SAR satellites emit successive pulses of electromagnetic radiation to measure the signal reflected off the Earth's surface. The incident signal interacts with the elements on the terrain and then is backscattered and measured by the radar according to the sensor frequency, the angle of incidence, and the geometry and dielectric properties of the target (Ulaby, 1982; Ulaby et al., 1981). Sentinel-1 satellites operate at C-band, with a central frequency of 5.405 GHz with different acquisition modes and product types available. The emitted microwaves are horizontally (H) or vertically (V) polarized, then the sensor measures the backscatter in the same (copolar) or orthogonal (cross-polar) polarization. In this study, the Interferometric Wide Swath (IW) mode is employed and hence two different polarization channels (i.e., VH and VV) will be available.

Satellite imagery either with passive or active sensors has already been used in marine science for many applications (Migliaccio et al., 2022), such as Iceberg detection (Marino et al., 2016; Soldal et al., 2019), ship detection (Iervolino et al., 2019), flood detection (Fichtner et al., 2023) and aquaculture monitoring (Detoni et al., 2023) and detection (Ballester-Berman et al., 2018; Marino et al., 2019). Concerning the latter, Ottinger et al., (2017) showed that images collected in this way can be used to detect aquaculture ponds in some river deltas in China and Vietnam, using high-resolution optical images to validate the results. We aim to detect aquaculture structures (i.e. not pounds) based only on SAR data, as optical data for specific periods can be hard to obtain. Kurekin et al., (2022) used a similar approach but applied to detect coastal aquaculture sites in the Philippines. Optical images from the Sentinel-2 mission were used to differentiate between land and sea.

Validation was done by mixing historical records of optical images and in-situ observations. Prasad et al. (2019) also used optical imagery as a supporting method but applied an object-based classification methodology adapted to the particular shape of aquaculture fish ponds. All these previous works used a median operator along the time dimension to isolate the dominant targets in an area, proving that it can be very effective for this work. Also noteworthy is the limited spatial analysis, as they processed very specific areas.

Our work here aims to develop a methodology capable of mapping European aquaculture compounds by using image analysis and machine learning. This mapping is generated from freely available radar data of satellite imagery from the Copernicus program, in the expectation that automatic mapping will speed up the rate at which aquaculture distribution estimates can be made, making it possible to monitor areas where official data is not available or not accurate.

2. Material and methods

This section describes the pipeline followed from the acquisition of the data to the final classification. Fig. 1 serves as a graphical summary. First, data collected by the Sentinel-1 satellites (Torres et al., 2012) was downloaded to a local repository (sec. 2.1). Then, these images were preprocessed employing open-source ESA Sentinel Application Platform (SNAP) software to obtain calibrated, despeckled, and geocoded images (sec. 2.2). Once the images were preprocessed, a temporal-wise median was computed for each pixel, to merge them and delete unwanted noise (sec 2.3). The iDPolRAD algorithm (Marino et al., 2016) (sec 2.4) and a posterior classifier were applied to the images to detect the presence of aquaculture sites (sec. 2.5).

2.1. Acquisition of data from selected areas

Five areas of interest within Western Europe were selected for the study (Fig. 2). The main reason for choosing these areas was that data on the actual placement of aquaculture was available (Fernandes-Salvador et al., 2021). That information was in the form of polygons or points in shapefiles. The polygons provide the exact area dedicated to aquaculture in each area, while the point informs of the presence of one or more aquaculture structures without providing any further information on their distribution.

The Sentinel-1A&B satellites, which were used in this study, collect data more frequently over Europe and other areas of interest so there is a higher temporal density of data for these areas (Torres et al., 2012). The SAR images employed were downloaded from the Copernicus Data Space Ecosystem (CDSE), using the Alaska Satellite Facility (ASF) Data Search as an alternative mirror when certain products were not available. APIs provided by CDSE and ASF were used to automate the download of products specifying the area of interest and time span of this study. The images were acquired in the Interferometric Wide Swath (IW) mode with the Ground Range Detected High resolution (GRDH) format, whose spatial resolution is 20x22 meters (range and azimuth, respectively) and a swath width of 250 km.

2.2. SAR image preprocessing

SAR satellite data preprocessing involves a series of procedures designed to correct signal artifacts, improve image quality, and extract features. This step is crucial to ensure accurate and reliable data. The European Space Agency (ESA) developed an open-source Earth observation analysis tool that can automate all the preprocessing. This toolbox is the Sentinel Applications Platform (SNAP) which integrates various tools and APIs to facilitate the view and processing of remotely

¹ https://dataspace.copernicus.eu/.

² https://search.asf.alaska.edu.

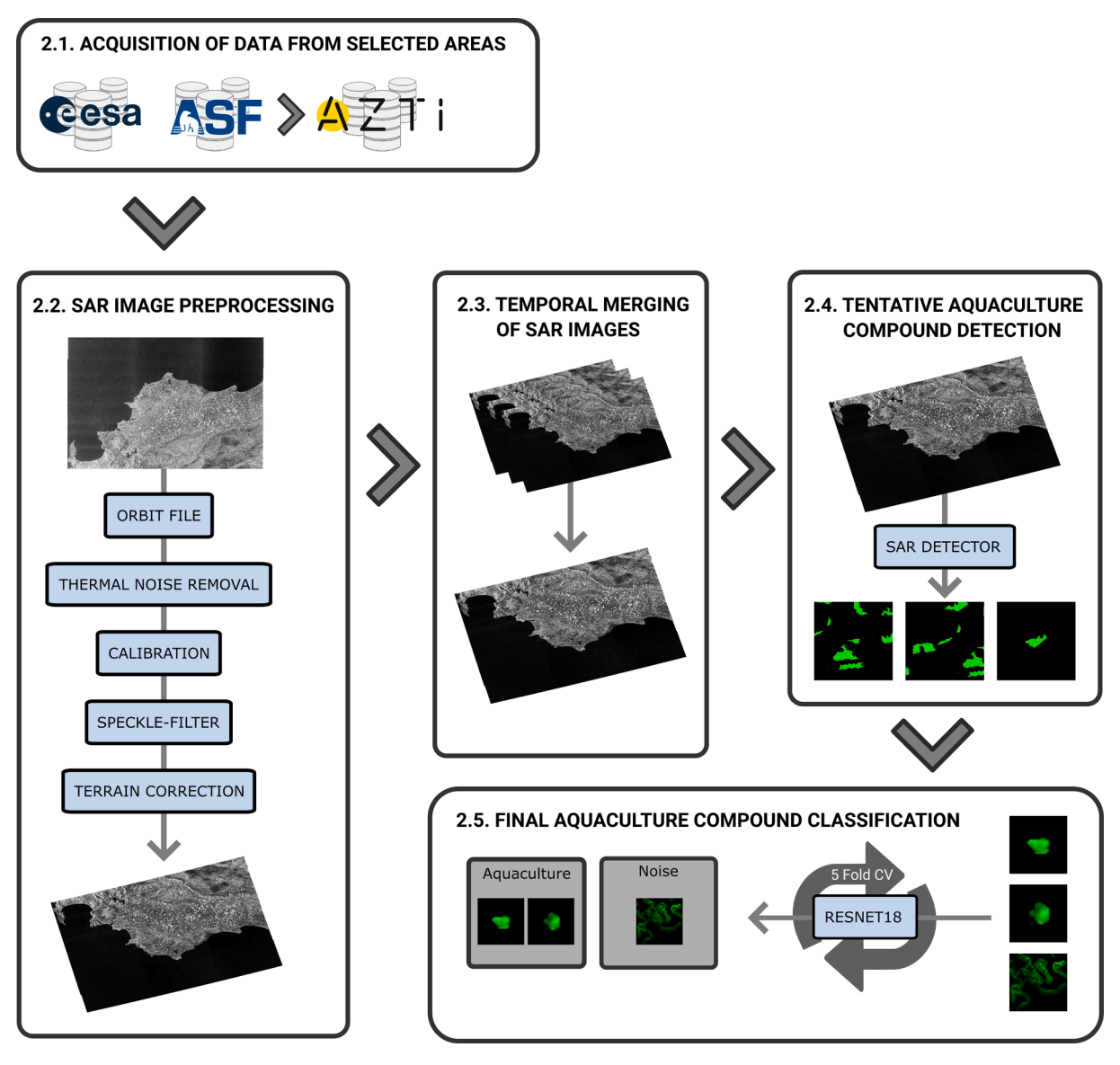


Fig. 1. Diagram summarizing the methodology of this study. See the paragraph above for a summary of the figure.

sensed data (Zuhlke et al., 2015). Using the programming language Python and some libraries that employ SNAP's APIs, the whole pipeline from data filtering and selection to preprocessing can be automated. The files generated after each preprocessing step greatly increased in size, so only the final file was saved. This file includes the images for the VV and VH polarizations, and the latitude, longitude, and elevation layers of each pixel. SNAP has many formats available to export the data, but the GeoTIFF format was chosen as it is a well-established standard and compatible with most GIS software. The process was based on the standard preprocessing of Sentinel-1 data (Filipponi, 2019). We divided it in five distinct steps.

- Apply Orbit-File. The metadata of a SAR product contains orbit state vectors to provide accurate satellite position and velocity information. However, these vectors are not accurate and can be improved with precise orbital files calculated after the generation of the product.
- 2) **Thermal Noise Removal.** System-induced thermal noise can affect radar signals, especially in the cross-polar channel. This stage reduces thermal noise by employing product annotations.
- Calibration. SAR calibration is used to make the value of the pixels proportional to the radar backscatter. The typical method used to

- generate the products does not include radiometric corrections, so significant bias remains. This correction is also necessary to compare SAR images acquired with different satellites or acquired from the same satellite but at different times.
- 4) **Speckle-Filter.** Interference among many elementary scattering centers inside the same resolution cell occurs due to the coherent nature of the SAR image formation process (Goodman, 1976). These interferences can be constructive or destructive, leading to image quality degradation by a granular noise which is called *speckle*. The boxcar (smoothing) filter has been proven to yield reasonable results for the present application (Ballester-Berman et al., 2018).
- 5) Terrain-Correction. Distances are distorted in the SAR product due to topographical variations of the scene and the tilt of the satellite. Data from targets not directly located at the satellite's nadir will have some distortion. Terrain correction is used to compensate for these distortions. In addition, this step geocodes the SAR image.

2.3. Temporal merging of SAR images

A major problem of employing radar imagery for target detection such as aquaculture structures, is the potential ambiguity of the detection with other types of structures also present in the ocean (i.e., ships,

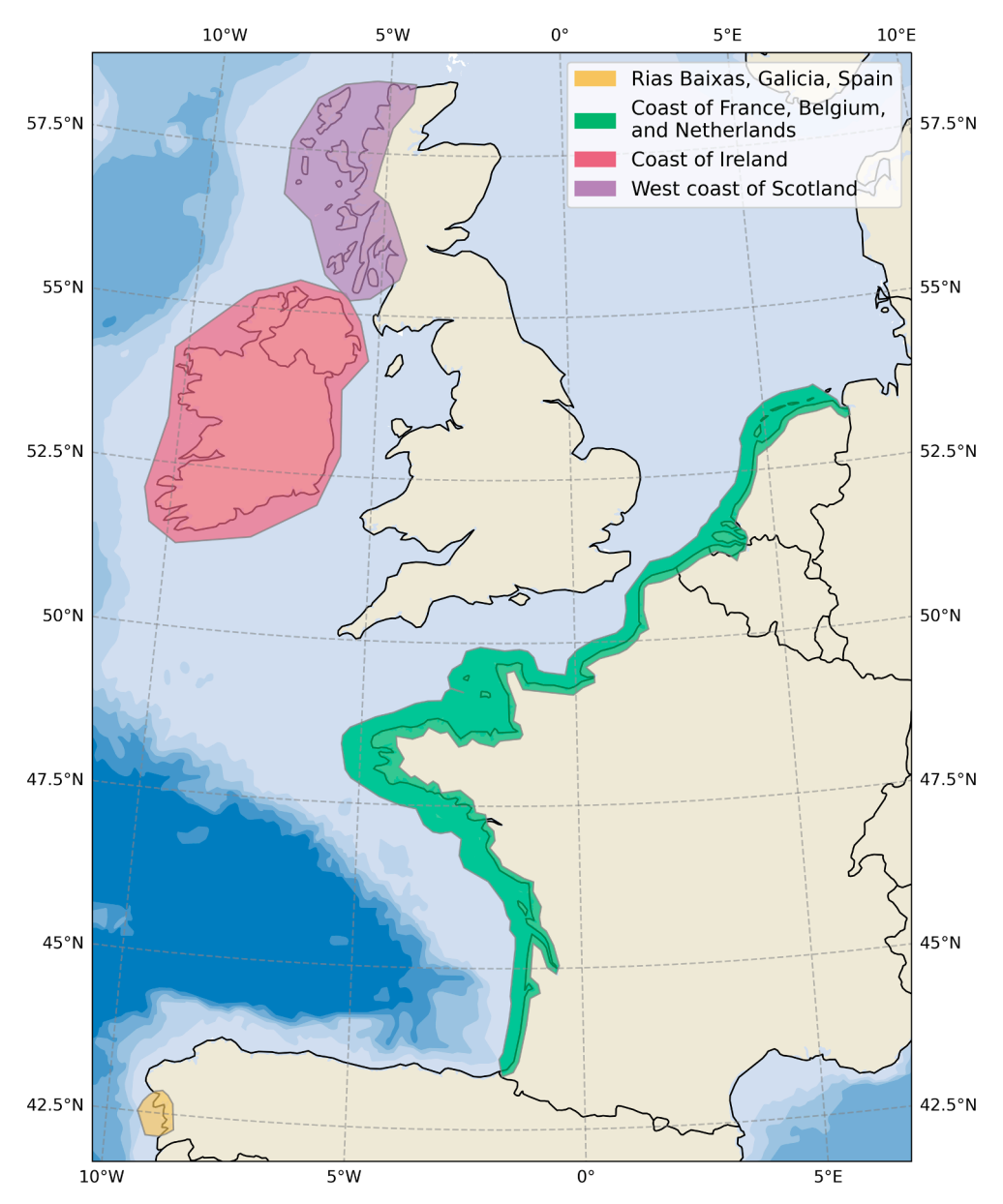


Fig. 2. The areas of the Atlantic Ocean that have been selected for this work.

oil rigs, wind farms, drifting objects, etc.). These moving objects can be considered as noise in a sequence of images. To eliminate them, a temporal median of each pixel was calculated by merging multiple products of the same area (Kurekin et al., 2022). For this purpose, two date ranges were selected. The first, from August 1, 2021, to August 31, 2021, and the second, from June 1, 2023, to June 30, 2023. This way, most of the noise-like artifacts caused by transient objects were removed and only static objects were retained.

Adverse weather conditions causing ocean waves are known to increase the backscattering power (Cloude, 2009; Lee & Pottier, 2009). Assuming that these conditions are not permanent, the unwanted high backscattering that causes the bright pixels can also be treated as noise and removed before applying the detection algorithm. The sea state during the selected periods was analyzed to check if there were any major storms during these periods. To do this, the mean and standard deviation of the Significant Wave Height (SWH) was taken as a reference. The number of products and sea conditions in the date ranges for each of the selected areas are shown in Table 1. The sea surface conditions were determined using data from Copernicus Marine Services, accessed through the Copernicus Marine Toolbox API. SWH data from

Table 1

Number of products downloaded and significant wave height data (mean and standard deviation) for each of the areas in the study during the selected time periods.

Area	Time period					
	2021/08/01 - 2021/08/31		2023/06/01 - 2023/06/30			
	Products	SWH	Products	SWH		
Galicia	40	1.17 m \pm 0.44 m	19	$0.92~\mathrm{m}\pm0.38~m$		
France	310	$0.96~{ m m}\pm0.62~{\it m}$	152	0.73 m \pm 0.41 m		
Ireland	201	$1.07~\mathrm{m}\pm0.85~m$	98	0.87 m \pm 0.8 m		
Scotland	160	0.84 m \pm 0.76 m	72	0.57 m \pm 0.55 m		

Ireland, Scotland, and the northern part of France were obtained using the Atlantic-European North West Shelf-Wave Physics Reanalysis product (European Union-Copernicus Marine Service, 2020), while the Mediterranean Sea Waves Reanalysis product (Korres et al., 2021) was used in Galicia and the southern part of France. The data suggest that there was no major storm during these time periods and that all sites

have approximately the same conditions, although the products from 2023 have slightly smaller waves. Based on the sea state codes of the World Meteorological Organization, the sea condition was primarily slight with intermittent moderate seas, which did not hinder the detection capabilities of Sentinel-1 data. The data in Table 1 also shows that the number of products decreased by approximately 50 % from 2021 to 2023. This is because one of the two Sentinel-1 constellation satellites, Sentinel-1B, failed between late 2021 and mid-2022.

The merged products were used as input for the detection stage, but first, all non-marine areas are masked from the GeoTIFF. Once the product has been preprocessed and the land has been discarded, the detection of aquaculture zones begins.

2.4. Tentative aquaculture compound detection

The intensity Dual-Polarization Ratio Anomaly Detector (iDPolRAD) algorithm was used to detect aquaculture zones. This algorithm was developed to detect icebergs using Sentinel-1 observations (Marino et al., 2016) and it is based on the idea that an object emerging from the surface will produce an anomaly in the volume scattering, so it searches for areas of high contrast between the two polarization channels in small windows of the image. This idea is driven by the theoretical aspects covered in radar polarimetry which studies the interaction of electromagnetic waves with matter. Fig. 3 illustrates the fundamental scattering mechanisms. It must be noted that the contribution of any of those mechanisms depends upon the specific polarization state and the geometry, orientation, size, and material making up the target under consideration. For further details on radar scattering processes, see (Cloude, 2009; Lee & Pottier, 2009).

Once the iDPolRAD detection algorithm has been applied, it is necessary to classify the detections. This classification aims to separate possible aquaculture zones from artifacts that remain in the image. These artifacts can be caused by harbors, areas where the tide changes a lot, or other types of structures related to human activity. To perform this classification, it is necessary to define certain parameters, such as the minimum value returned by the algorithm that will be considered as a detection and the maximum distance at which two detections can be found to consider them as part of the same aquaculture site. For this purpose, a test area was selected where the real data of aquaculture zones are available. The area chosen to find the optimal parameters was four of the five estuaries of Rías Baixas in Galicia, Spain (Fig. 2, area 1). Specifically, the estuaries of Ría de Vigo, Ría de Pontevedra, Ría de Arousa, and Ría de Muros e Noia. This area measures approximately 80 km from north to south and 40 km from east to west, about 3,200 square kilometers. Galicia is the largest producer of mussels through aquaculture in Spain (Labarta & Fernández-Reiriz, 2019), so it is not surprising that more than 3,000 aquaculture sites are located within these estuaries. The large number of aquaculture sites in the area, their precise mapping, and the placement of the structures above the water made this area ideal for conducting the parameter selection experiment.

2.5. Final aquaculture compound classification

The final discrimination between noise and aquaculture zones was performed using a deep learning approach. More specifically, we assessed the performance of three neural network architectures, namely ResNet18, ResNet34 (He et al., 2016), and a custom implementation of Vision Transformers (ViT) (Gani et al., 2022). These architectures, characterized by 11 million, 21 million and 2.8 million trainable parameters respectively, are relatively shallow, resulting in low computational costs for both training and execution compared to deeper models. The limited number of parameters also decreases the risk of overfitting, a concern that arises when a model's complexity surpasses the available training data (Gupta et al., 2018). Table 2 provides details on the used infrastructure and parameters. While all architectures showed similar performance in the conducted experiments, ResNet18 was selected based on a careful balance of the time spent to train it and the results obtained. The final model was implemented using FastAI's (PyTorch) ResNet18 architecture without pre-trained weights.

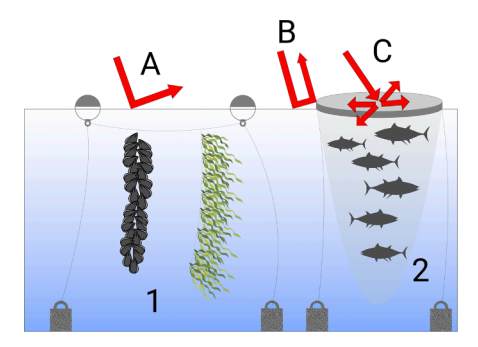
Given that the images generated in the previous steps varied in size due to the nature of the detection process, they were uniformly resized to 32x32 pixels to facilitate processing. Data augmentation techniques were employed, including random rotation within the [0, 360] degree range, random vertical and horizontal flipping, and zooming in the range of [1.0, 3.0]. These measures contribute to enhancing the model's robustness. Models were trained until convergence to ensure optimal performance.

3. Results

This section presents the results related to the selection of segmentation parameters to distinguish human platforms at sea. It also provides insights into the statistical performance of the classification model,

Table 2Parameters and the values that were tested during different runs and the ones that were used to train the final model.

Hyperparameter	Search space	Best assignment		
Number of epochs	1 – 1000	600		
Number of folds	4–5	5		
Model architecture	ResNet18, ResNet34, ViT	ResNet18		
Weight decay	0.1	0.1		
Batch size	4	4		
Other parameters	Value			
Computing infrastructure	Tesla V100 16 GB (x2)			
Number of search trials	15			
Search strategy	Manual Search			
Best validation accuracy	93 %			
Training duration	1 h 30 min – 3 h 45 min			
Validation	5-fold cross-validation			
Code, data and model Zenodo / GitHub (Lekunberri et al., 2023)				



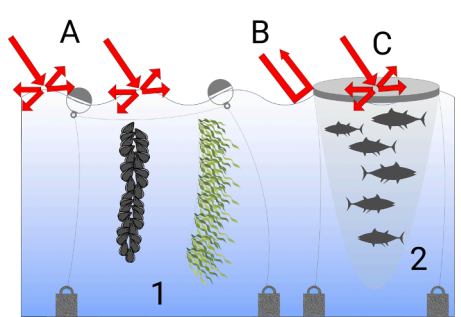


Fig. 3. Scattering of electromagnetic waves on different sea surface conditions and aquaculture elements. Left figure: calm sea at the surface. Right image, rough sea. Types of scattering. a) Surface scattering, b) Double-bounce scattering, c) Volume scattering. In this example, fish farms (2) can be located using SAR imagery, while mussel and kelp farms (1) can't.

focusing on its training to distinguish aquaculture sites from noise and other platforms, and its testing against ground truth data, sourced from national authorities and visually verified aquaculture locations.

3.1. Tentative aquaculture compound detection

The optimal segmentation parameters for SAR-derived images were determined through an iterative search. This search considered the number of products to merge, the maximum distance between neighboring sites, and a threshold for discarding points with the weakest backscatter. To assess the effectiveness of different parameter combinations, the Intersection over Union (IoU) between the detections and ground truth data was calculated as the evaluation criterion. The IoU quantifies the overlap by measuring the area of the predicted aquaculture zone that intersects with the ground truth, divided by the sum of both areas. A resulting IoU value of 0 indicates no overlap, while a value of 1.0 reflects a perfect match. Several runs were conducted using data spanning up to 21 weeks, but after 6 weeks of merging there was no significant improvement in the maximum reported IoU. Fig. 4 shows the data obtained by merging 6 weeks' worth of data.

For the detection threshold, a range of values from 0 to 10 in increments of 1 were tested, where 0 indicates the use of all detections and 10 implies the discarding of the weakest 10 %. A similar approach was taken with the maximum distance required to consider two detections as neighbors, ranging from 150 to 350 m with an increment factor of 10 m. The optimal configuration was achieved at a maximum distance of 350 m with a threshold of 1, resulting in an IoU of 0.5211.

3.2. Final aquaculture compound classification

After the segmentation process, the tentative aquaculture areas were classified using a deep learning model. As previously mentioned, two ResNet and one ViT architecture were tested. The deepest of the convolutional networks, ResNet34, overfitted in a few epochs and failed to provide any useful results. It appears that, despite its relatively small size, this architecture is too large for our data. In contrast, the other two architectures, ResNet18 and ViT, achieved good results. Table 3 shows some statistics to compare both networks where, in all of the metrics, the ResNet18 showed superior performance but was statistically significant in F1 score, accuracy, and specificity.

Another factor that was considered during the training process was whether to use a network with pretrained weights or not. The confusion matrices in Fig. 5 provide a comparative analysis of the deep learning model using those two approaches: pre-trained and non-pre-trained weights. The non-pre-trained approach (Fig. 5b) shows superior accuracy (90 % compared to 59 %), particularly excelling in the classification

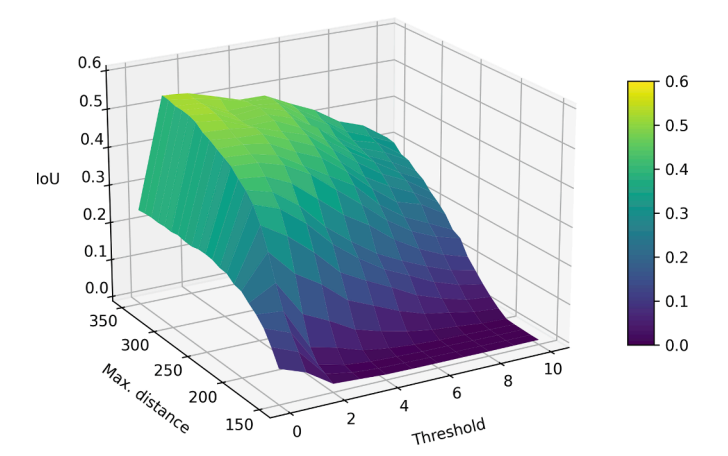


Fig. 4. All possible values for a given area plotted as a 2D surface. This specific case belongs to the merging of 6 weeks' worth of data.

Mean and standard deviation for ResNet18 and ViT, the two architectures that showed similar results. Paired sample *t*-test calculated p < 0.05 (*), p < 0.01 (†) and p < 0.001 (†).

Architecture	F1 Score*	Accuracy*	Sensitivity	Specificity*
ResNet18	0.89 ± 0.02	$0.89 \pm 0.02 \\ 0.85 \pm 0.02$	0.89 ± 0.04	0.90 ± 0.03
ViT	0.83 ± 0.03		0.84 ± 0.06	0.83 ± 0.03

of aquaculture (93 %). While pre-trained networks demonstrate higher accuracy in noise classification (92 %), this approach performs poorly with targeted aquaculture images (27 %), resulting in a 73 % misclassification of aquaculture sites classified as noise. In contrast, the non-pre-trained approach (Fig. 5b) not only achieves superior overall accuracy (90 %) but also maintains a balanced performance between aquaculture (93 %) and noise (87 %). Moreover, the misclassification of aquaculture sites as noise is very rare (7 %) in this non-pre-trained approach. A trade-off exists, where 13 % of noise is incorrectly classified as aquaculture sites. Despite this, the model can be considered to have competitive performance and a postprocessing step can be employed to filter out some of this noise.

The selected model demonstrated good performance, but its ability to generalize to new aquaculture areas may be constrained by the considerable diversity of structures across regions. To assess the network's generalization power with new sites, cross-validation was conducted, treating each of the five areas as a subset for testing. We followed a leave-one-out strategy, where one site was reserved for testing while the model learned from the rest. However, the results revealed high rates of false positives and false negatives, with accuracies not surpassing those of random classification.

Similar results persisted when sites were paired for testing and learning with another two sites, as outlined in Table 4. The models showed accuracies comparable to random chance (41 \pm 12 %), consistent with sensitivities and specificities of either 0 % or 100 %. This lack of generalization power to new areas can be attributed to the limited number of available training images in each aquaculture area (56 in France, 131 in Galicia, 83 in Ireland, and 331 in Scotland), coupled with the variability in types of aquaculture sites and cage geometry.

Investigating the ineffectiveness of training data separation based on geographical areas, an analysis of the model's learning behavior was conducted to discern whether the issue stemmed from the diverse nature of aquaculture types across regions. To visually represent this behavior, we employed the Uniform Manifold Approximation and Projection (UMAP) technique, known for its ability to reduce data dimensionality and facilitate visualization (McInnes et al., 2020). Fig. 6 showcases the application of UMAP to comprehend the model's performance, with data color-coded based on their respective areas of origin.

The transformed data reveals four elongated clusters, each depicted with a pie chart illustrating the distribution of areas within. Notably, the cluster situated in the bottom left corner stands out due to its smaller size (comprising 61 elements) and a predominant concentration of images from Galicia (74 %). Images from other regions within this cluster are mostly from Scotland (23 %), which also maintains a substantial presence in the remaining clusters. In contrast, the other three clusters exhibit similar area distributions, with France consistently accounting for around 10 % and Ireland for around 15 %. While Galicia and Scotland show varying percentages within these clusters, the sum of both regions remains stable at approximately 75 %. These percentage distributions correspond closely to the proportion of areas represented in each geographical zone. While these findings will be further discussed, they offer valuable insights into the model's generalization capabilities.

Understanding the different parameters of the model with regard to aquaculture and noise classification is crucial to assess the model's performance. However, the primary objective of this work is to identify actual aquaculture areas. Fig. 7 shows a map centered on the Rías Baixas region of Galicia. As can be observed, the data used as ground truth

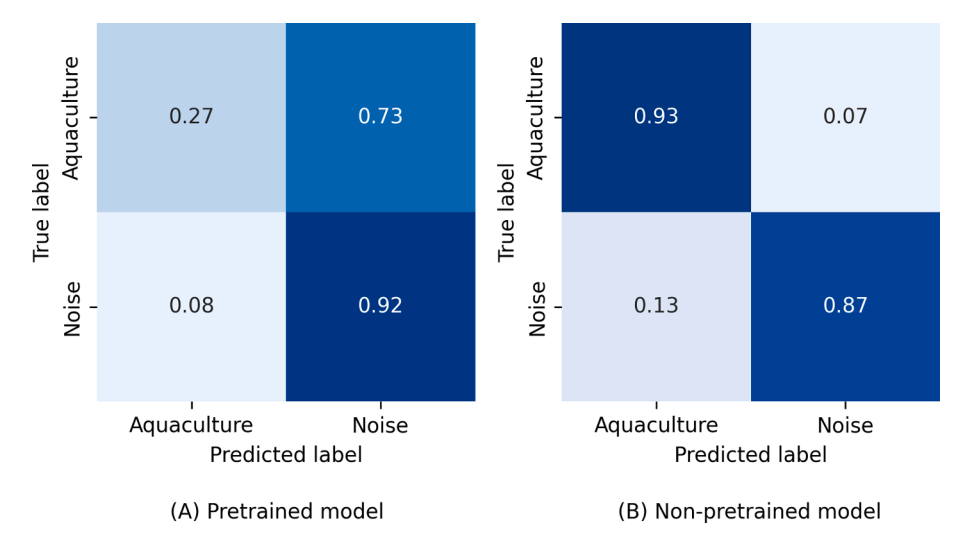


Fig. 5. Confusion matrices for the two models. The vertical axis represents the actual label of the image, and the horizontal axis represents the label predicted by the model.

Table 4Statistics for each of the combinations in which models were trained. The areas were grouped in pairs in each run.

	•			
Train areas	Validation areas	Accuracy	Sensitivity	Specificity
Ireland, Scotland	France, Galicia	34.2 %	100.0 %	0.0 %
Galicia, Scotland	France, Ireland	53.3 %	0.0 %	100.0 %
Galicia, Ireland	France, Scotland	33.3 %	0.0 %	100.0 %
France, Scotland	Galicia, Ireland	39.8 %	95.0 %	10.0 %
France, Ireland	Galicia, Scotland	58.7 %	0.0 %	100.0 %
France, Galicia	Ireland, Scotland	26.9 %	0.0 %	100.0 %
Mean and SD:		$\begin{array}{c} 41\% \pm 12.4 \\ \% \end{array}$	$32.5\%~\pm\\50.4~\%$	$68.3\%~\pm$ $44.9~\%$

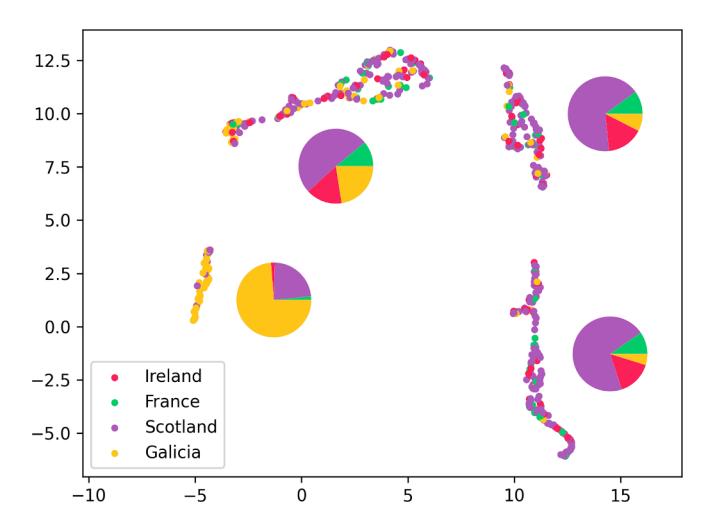


Fig. 6. UMAP visualization of the embeddings of the trained neural network. A pie chart displaying the relative abundance of each area.

around $42.5^{\circ}N$ $8.9^{\circ}W$ is inaccurate, as the detected (and manually verified) aquaculture area is much larger than officially reported. This provides evidence of the necessity of a real-time data tool like the one

presented in this work. Most of the green polygons, indicating true aquaculture zones, contain one or more green points, indicating aquaculture zones detected by the trained model. It is important to note that the number of points per polygon is not an indicator of the model's confidence in its prediction. Instead, it suggests that the model struggled to group these detections into a single entity. Expanding the image with offshore data introduces a substantial amount of noise, but as open ocean areas do not contain aquaculture cages, they can be cropped.

4. Discussion

This work proposes a method for automatic detection and classification of aquaculture zones based on satellite SAR data and deep learning. The system offers full automation, enabling the monitoring of regional status evolution by defining specific areas. Given the periodic renewal of Sentinel-1 radar imagery, which is freely available, this methodology provides a cost-effective means to track aquaculture activity. To enhance the accuracy of detection, the merging of multiple radar detections was proposed, employing a temporal median to discard moving objects and noise, thereby improving upon previous approaches (Ballester-Berman et al., 2018; Marino et al., 2019). Adjustments in the number of images to be merged were made based on temporal resolution, ensuring adaptability to detect changes occurring over different time scales. Typically, an average of 3 to 5 images were used. In the final stage, a deep learning approach was employed for image classification, reaching an accuracy of 93 %, surpassing results in other works such as Ottinger et al., (2017) and Kurekin et al., (2022).

One of the major limitations encountered in this study revolves around the diversity of structures used for different aquaculture species and their corresponding geometries, which can be broadly categorized into two groups: (1) structures partially above sea level and (2) structures completely submerged (Chu et al., 2020). The former, commonly employed for fish or bivalve breeding and anchored to the seabed, are the ones that we were able to detect using SAR data. Any of these structures will interact and return a signal to the satellite, even if it is smaller than 20x22m (Sentinel-1 resolution). The returned signal is an average that includes the interactions of the entire resolution cell. Since the signals returned by the water-structure interaction are much larger than those returned by the water surface, this average is normally sufficient to detect such structures. The second type of structures stay entirely underwater either due to intentional installation to remain submerged continuously, or temporarily during tides or specific sea conditions. The placement of these structures renders remote sensing via SAR impractical, as electromagnetic waves interact with the water

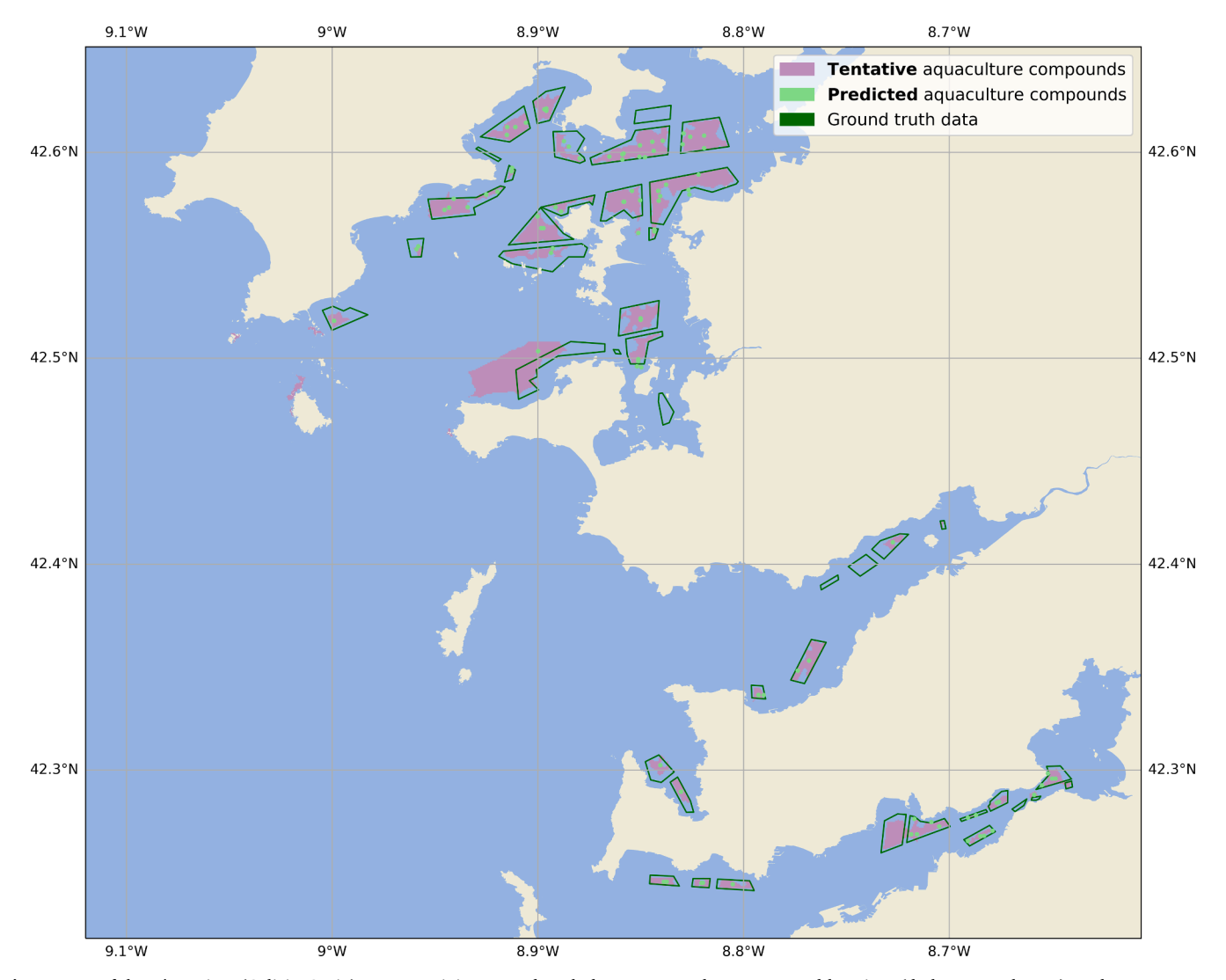


Fig. 7. Map of the Rías Baixas (Galicia, Spain) area containing ground truth data on aquaculture compound locations (dark green polygons). Red areas are areas detected with iDPolRAD and clustered, marked as possible aquaculture compounds. Light green points are the areas where the final model predicted that there is actual aquaculture activity.

surface and do not penetrate deeply enough (i.e. a few millimeters) to detect these submerged structures.

Our tests with Sentinel-1C-band data revealed that these specific structures are challenging to discriminate from sea clutter, regardless of the VH or VV channels used. Detection strongly relies on favorable sea conditions as well as the angle formed by the aquaculture compound to the satellite track (Murata et al., 2023). Transitioning to a higher resolution mode, such as the Single Look Complex (SLC) Wave Mode (2.0x4.8 m, in range and azimuth, respectively), or even leveraging very high-resolution capabilities such as those offered by the X-band Capella Space satellite constellation (Stringham et al., 2019) with 0.6x0.63 m resolution, could potentially overcome the limitations associated with these particular marine structures. A small-scale experiment using these high-resolution commercial satellites, confirmed successful detection. However, due to our commitment to open and free data accessibility, we opted not to pursue this approach. Furthermore, these commercial solutions lack the temporal and spatial coverage provided by Sentinel-1 satellites. Nonetheless, the methodology presented can be feasibly applied to proprietary data.

Regarding the different model architectures used, ResNet18 and ViT achieved better results than ResNet34. The originally proposed smallest ViT architecture (Dosovitskiy et al., 2021) is more complex (i.e. it has more trainable parameters) than the deepest ResNet (even deeper than

the one used here), thus, making it more challenging to use this architecture in cases with small datasets. The large amount of data and computational resources needed to train one of those ViTs, encouraged the development of lighter versions of this architecture (Gani et al., 2022; Tan, 2024). Given that the ResNet34 was too complex for use, we chose one of these implementations of ViT because of the relative simplicity. In our case, both trained models produced satisfactory results, with a mean F1 score of 0.89 for the ResNet18 and 0.83 for the ViT. The ResNet18, due to its bigger number of parameters, required a longer training period in terms of both epochs and training time to reach convergence but still was selected as the final model because of its slightly better results. Further work should be conducted with these novel and simplified ViT architectures to better exploit their potential.

Pre-trained models are frequently favored due to their shorter training times and often superior performance compared to non-pre-trained models. Typically, this technique is applied when images from both (pre-training and re-training) datasets belong to the same domain, but this assumption does not always hold true. Biomedical (Kieffer et al., 2017; Shallu & Mehra, 2018; Tajbakhsh et al., 2016) and agricultural (Ihsan Aquil & Wan Ishak, 2021; Sahu et al., 2020) imaging are two domains where models pre-trained with general datasets exhibit better performance than their non-pre-trained counterparts. Satellite imagery, encompassing both optical and non-optical spectrum data, is no

exception, with applications reporting successful outcomes (Gonzales & Sakla, 2019; Zou & Zhong, 2018). However, in this specific case, the pretrained models demonstrated poor performance.

Several factors may contribute to this outcome, but a primary reason could be the disparity between the images used for pre-training, which were RGB images captured in the visible spectrum, and our images composed of values dependent on the interaction of electromagnetic waves with the target in the microwave regime (Ulaby, 1982; Ulaby et al., 1981). The variability in cage structure is also partially responsible for the model's difficulty in generalizing. Even when the locations of aquaculture farms are known, processing the area and cropping the images to generate training data for the model is essential. This involves identifying the aquaculture farm, distinguishing it from possible noise, and manually cropping the area. Despite being a time-consuming process, dedicating more time to manual data collection could likely enhance the model's generalization power. The balance between time spent and results achieved is deemed satisfactory.

Despite the generalization limitations inherent in this study, to the best of our knowledge, this marks the first instance of automatically detecting and classifying large above-water aquaculture compounds at the macroscale using only SAR data. Prominent studies by Ottinger et al., (2017) and Kurekin et al., (2022) achieved accuracies of 83 % and 72 %, respectively, yet they rely on optical images in a supplementary manner and have been tested in smaller regions. While some proof of concept for detection based solely on SAR data exists (Ballester-Berman et al., 2018; Marino et al., 2019), these previous studies primarily focused on assessing whether the structures could be detected. However, they did not delve into the classification aspect to distinguish aquaculture sites from noise and other structures or accomplish the full mapping of entire areas with spatial ground truth verification.

Given that the distribution of aquaculture activity is not freely and readily available (Fernandes-Salvador et al., 2021) such information becomes imperative to advance beyond the current state-of-the-art in scientific and management research, including identifying pressures and spatial planning (Coccoli et al., 2018). While our results are cost-effective, promising, and potentially useful, they are only estimations based on remote sensing data and cannot replace proper monitoring by relevant institutions. As previously mentioned, data from satellites with better resolution could improve the results even more. Still, regular updates of the data and its availability will always be more accurate and allow for better management of marine resources.

5. Conclusions

The Copernicus program provides an excellent opportunity to collect data from the earth's surface in a relatively short period. This study proposes the integration of the data collected by the Sentinel-1 satellites in a pipeline that uses artificial neural networks to automatically identify aquaculture zones in selected regions. The findings of this study were as follows:

Merging data from the same areas but captured during different dates represents an effective approach for noise reduction and discarding moving objects in each image. In this study, 6 weeks' worth of data has shown the best results for the initial detection, but this can change depending on the time the satellite takes to revisit the area.

The iDPolRAD algorithm, initially developed for iceberg detection, is an efficient method to detect aquaculture compounds in SAR images. Although it also captures some noise, it can be easily discarded in consequent steps.

Satisfactory results are achieved in differentiating aquaculture from noise (see Table III for detailed scores) in the areas where the model has been trained. The limited number of available training images and the variability in types of aquaculture sites may be responsible for the lack of generalization capabilities. Also, we plan to further

investigate the use of smaller ViT architectures with databases like

Sentinel-1C-band data showed that some specific structures are difficult to distinguish from the noise caused by the sea. The detection depends on favorable sea conditions and the angle between the aquaculture compound and the satellite track. Switching to data with higher resolution could potentially address these limitations.

CRediT authorship contribution statement

Xabier Lekunberri: Writing – original draft, Software, Methodology, Investigation, Data curation. J. David Ballester-Berman: Writing – review & editing, Methodology, Investigation, Conceptualization. Ignacio Arganda-Carreras: Writing – review & editing, Software, Methodology. Jose A. Fernandes-Salvador: Writing – review & editing, Supervision, Conceptualization.

Declaration of competing interest

The authors declare that they have no known competing financial interests or personal relationships that could have appeared to influence the work reported in this paper.

Data availability

We have shared the link to the data in the manuscript.

Data and code are available at https://zenodo.

org/doi/10.5281/zenodo.10354236 (Lekunberri et al., 2023).

Acknowledgments

Xabier Lekunberri has benefited from a Ph.D. grant from the IKER-TALENT Programme of the Department of Economic Development, Sustainability, and Environment Department of the Basque Government. This work was partly funded by the European Union's Horizon 2020 research and innovation program under grant agreements No 101136674 (OptiFish), No 869300 (FutureMARES project) and No 862428 (Mission Atlantic project). It has been also supported by Bio-Boost + project within the Biodiversa + European Biodiversity Partnership program. Funded by the European Union. Views and opinions expressed are however those of the author(s) only and do not necessarily reflect those of the European Union or Fundación Biodiversidad. Neither the European Union nor the granting authority can be held responsible for them. The authors wish to express their gratitude to the European Space Agency for providing the SNAP software and for processing and distributing the Sentinel-1 data that was downloaded from the Copernicus Open Access Hub and the Alaska Satellite Facility's data portal. This work is partially supported by grant GIU19/027 funded by the University of the Basque Country (UPV/EHU), and grant PID2021-1267010B-I00 funded by the Ministerio de Ciencia, Innovación y Universidades, AEI, MCIN/AEI/10.13039/501100011033, and by "ERDF A way of making Europe". This paper is contribution No 1232 from AZTI, Marine Research, Basque Research and Technology Alliance (BRTA).

References

Alleway, H.K., Gillies, C.L., Bishop, M.J., Gentry, R.R., Theuerkauf, S.J., Jones, R., 2019. The Ecosystem Services of Marine Aquaculture: Valuing Benefits to People and Nature, Bioscience 69 (1), 59–68. https://doi.org/10.1093/biosci/biv137.

Avdelas, L., Avdic-Mravlje, E., Borges Marques, A.C., Cano, S., Capelle, J.J., Carvalho, N., Cozzolino, M., Dennis, J., Ellis, T., Fernández Polanco, J.M., Guillen, J., Lasner, T., Le Bihan, V., Llorente, I., Mol, A., Nicheva, S., Nielsen, R., van Oostenbrugge, H., Villasante, S., Asche, F., 2021. The decline of mussel aquaculture in the European Union: Causes, economic impacts and opportunities. Rev. Aquac. 13 (1), 91–118. https://doi.org/10.1111/raq.12465.

Ballester-Berman, J. D., Sanchez-Jerez, P., & Marino, A. (2018). Detection of aquaculture structures using Sentinel-1 data. EUSAR 2018; 12th European Conference on Synthetic Aperture Radar, 1–4.

- Borgeaud, M., Drinkwater, M., Silvestrin, P., Rast, M., 2015. Status of the ESA earth explorer missions and the new ESA earth observation science strategy. IEEE International Geoscience and Remote Sensing Symposium (IGARSS) 2015, 4189-4192. https://doi.org/10.1109/IGARSS.2015.7326749.
- Chu, Y.I., Wang, C.M., Park, J.C., Lader, P.F., 2020. Review of cage and containment tank designs for offshore fish farming. Aquaculture 519, 734928. https://doi.org/ 10.1016/j.aquaculture.2020.734928
- Cloude, S., 2009. Polarisation: Applications in Remote Sensing. Oxford University Press. //doi.org/10.1093/acprof:oso/9780199569731.001.0001
- Coccoli, C., Galparsoro, I., Murillas, A., Pınarbaşı, K., Fernandes, J.A., 2018. Conflict analysis and reallocation opportunities in the framework of marine spatial planning: A novel, spatially explicit Bayesian belief network approach for artisanal fishing and aquaculture. Mar. Policy 94, 119-131. https://doi.org/10.1016/j marpol.2018.04.015
- ESA Communications. (2012). Sentinel-1: ESA's Radar Observatory Mission for GMES Operational Services. ESA Communications.
- Detoni, A.M.S., Navarro, G., Garrido, J.L., Rodríguez, F., Hernández-Urcera, J., Caballero, I., 2023. Mapping dinoflagellate blooms (Noctiluca and Alexandrium) in aquaculture production areas in the NW Iberian Peninsula with the Sentinel-2/3 satellites. Sci. Total Environ. 868, 161579 https://doi.org/10.1016/j. scitoteny 2023 161579
- Dong, S., Liu, D., Zhu, B., Zhang, D., Wang, F., 2024. Practice assessment of integrated marine pond aquaculture for increasing benefits and reducing environmental pollution using an ecosystem modeling approach. Sci. Total Environ. 908, 168408 https://doi.org/10.1016/j.scitotenv.2023.168408.
- Dosovitskiy, A., Beyer, L., Kolesnikov, A., Weissenborn, D., Zhai, X., Unterthiner, T., Dehghani, M., Minderer, M., Heigold, G., Gelly, S., Uszkoreit, J., & Houlsby, N. (2021). An Image is Worth 16x16 Words: Transformers for Image Recognition at Scale (arXiv:2010.11929). arXiv. doi: 10.48550/arXiv.2010.11929.
- Erauskin-Extramiana, M., Chust, G., Arrizabalaga, H., Cheung, W.W.L., Santiago, J., Merino, G., Fernandes-Salvador, J.A., 2023. Implications for the global tuna fishing industry of climate change-driven alterations in productivity and body sizes. Global Planet, Change 222, 104055. https://doi.org/10.1016/j.gloplacha.2023.104055.
- European Union-Copernicus Marine Service. (2020). Atlantic- European North West Shelf-Wave Physics Reanalysis . doi: 10.48670/MOI-00060.
- FAO. (2020). The State of World Fisheries and Aquaculture 2020: Sustainability in action. FAO. doi: 10.4060/ca9229en.
- Fernandes, J. A., Mateo, M., M., Sagarminaga, Y., Lekunberri, X., Furey, T., Kozachenco, M., Pedreschi, D., Proud, R., Ostle, C., Shannon, L., Sink, K., Skein, L., Majiedt, P., Souza, V. A., Garcia Scherer, M. E., Gasalla, M. A., Ribeiro Gandra, T. B., Floeter, S. R., Bonetti, J., ... Chust, G. (2023). Maps of present ecosystem pressures (fishing, shipping, pollution and other). Zenodo. doi: 10.5281/ZENODO.7665526.
- Fernandes-Salvador, J.A., Davidson, K., Sourisseau, M., Revilla, M., Schmidt, W., Clarke, D., Miller, P.I., Arce, P., Fernández, R., Maman, L., Silva, A., Whyte, C., Mateo, M., Neira, P., Mateus, M., Ruiz-Villarreal, M., Ferrer, L., Silke, J., 2021. Current Status of Forecasting Toxic Harmful Algae for the North-East Atlantic Shellfish Aquaculture Industry. Front. Mar. Sci. 8 https://doi.org/10.3389 fmars 2021 666583.
- Fichtner, F., Mandery, N., Wieland, M., Groth, S., Martinis, S., Riedlinger, T., 2023. Timeseries analysis of Sentinel-1/2 data for flood detection using a discrete global grid system and seasonal decomposition. Int. J. Appl. Earth Obs. Geoinf. 119, 103329 https://doi.org/10.1016/j.jag.2023.103329.
- Filipponi, F., 2019. Sentinel-1 GRD Preprocessing Workflow. Proceedings 18(1), Article 1. https://doi.org/10.3390/ECRS-3-06201.
- Gani, H., Naseer, M., & Yaqub, M. (2022). How to Train Vision Transformer on Small-scale Datasets? (arXiv:2210.07240). arXiv. doi: 10.48550/arXiv.2210.07240.
- Geudtner, D., Gebert, N., Tossaint, M., Davidson, M., Heliere, F., Navas Traver, I., Furnell, R., & Torres, R. (2021). Copernicus and ESA SAR Missions. 2021 IEEE Radar Conference (RadarConf21), 1-6. doi: 10.1109/RadarConf2147009.2021.9455262.
- Gonzales, C., Sakla, W., 2019. Semantic segmentation of clouds in satellite imagery using deep pre-trained U-nets. IEEE Applied Imagery Pattern Recognition Workshop (AIPR) 2019, 1-7. https://doi.org/10.1109/AIPR47015.2019.91745
- Goodman, J.W., 1976. Some fundamental properties of speckle*. JOSA 66 (11), 1145-1150. https://doi.org/10.1364/JOSA.66.001145.
- Gupta, S., Gupta, R., Ojha, M., Singh, K.P., 2018. A Comparative Analysis of Various Regularization Techniques to Solve Overfitting Problem in Artificial Neural Network. In: Panda, B., Sharma, S., Roy, N.R. (Eds.), Data Science and Analytics. Springer, pp. 363-371. https://doi.org/10.1007/978-981-10-8527-7_30.
- He, K., Zhang, X., Ren, S., Sun, J., 2016. Deep Residual Learning for Image Recognition. IEEE Conference on Computer Vision and Pattern Recognition (CVPR) 2016, 770-778. https://doi.org/10.1109/CVPR.2016.90
- Hough, C., 2022. Regional review on status and trends in aquaculture development in
- Europe 2020. Food & Agriculture Org. https://doi.org/10.4060/cb7809en. Iervolino, P., Guida, R., Amitrano, D., & Marino, A. (2019). SAR Ship Detection for Rough Sea Conditions. IGARSS 2019 - 2019 IEEE International Geoscience and Remote Sensing Symposium, 505-508. doi: 10.1109/IGARSS.2019.8900332.
- Ihsan Aquil, M.A., Wan Ishak, W.H., 2021. Evaluation of scratch and pre-trained convolutional neural networks for the classification of Tomato plant diseases. IAES Int. J. Artif. Intellig. (IJ-AI) 10 (2), 467. https://doi.org/10.11591/ijai.v10.i2.pp467-
- Kieffer, B., Babaie, M., Kalra, S., & Tizhoosh, H. R. (2017). Convolutional neural networks for histopathology image classification: Training vs. Using pre-trained networks. 2017 Seventh International Conference on Image Processing Theory, Tools and Applications (IPTA), 1-6. doi: 10.1109/IPTA.2017.8310149.
- Korres, G., Ravdas, M., Zacharioudaki, A., Denaxa, D., & Sotiropoulou, M. (2021). Mediterranean Sea Waves Reanalysis (CMEMS Med-Waves, MedWAM3 system):

- MEDSEA_MULTIYEAR_WAV_006_012 (Version 1) . doi: 10.25423/CMCC/MEDSEA_ MULTIYEAR WAV 006 012.
- Kurekin, A.A., Miller, P.I., Avillanosa, A.L., Sumeldan, J.D.C., 2022. Monitoring of Coastal Aquaculture Sites in the Philippines through Automated Time Series Analysis of Sentinel-1 SAR Images. Remote Sens. (Basel) 14 (12), Article 12. https://doi.org/ 10.3390/rs14122862
- Labarta, U., Fernández-Reiriz, M.J., 2019. The Galician mussel industry: Innovation and changes in the last forty years. Ocean Coast. Manag. 167, 208-218. https://doi.org/ 10.1016/j.ocecoaman.2018.10.012
- Lee, J.-S., & Pottier, E. (2009). Polarimetric radar imaging: From basics to applications. CRC Press. doi: 10.1201/9781420054989.
- Lekunberri, X., Ballester-Berman, J. D., Arganda-Carreras, I., & Fernandes-Salvador, J. A. (2023). Automatic mapping of aquaculture activity in the Atlantic Ocean (CODE & DATA) (v1.0.0) [Computer software]. Zenodo. doi: 10.5281/ZENODO.10354236.
- Lotze, H.K., Tittensor, D.P., Bryndum-Buchholz, A., Eddy, T.D., Cheung, W.W.L., Galbraith, E.D., Barange, M., Barrier, N., Bianchi, D., Blanchard, J.L., Bopp, L. Büchner, M., Bulman, C.M., Carozza, D.A., Christensen, V., Coll, M., Dunne, J.P., Fulton, E.A., Jennings, S., Worm, B., 2019. Global ensemble projections reveal trophic amplification of ocean biomass declines with climate change. Proc. Natl. Acad. Sci. 116 (26), 12907-12912. https://doi.org/10.1073/pnas.1900194116
- Maire, E., Graham, N.A.J., MacNeil, M.A., Lam, V.W.Y., Robinson, J.P.W., Cheung, W.W. L., Hicks, C.C., 2021. Micronutrient supply from global marine fisheries under climate change and overfishing. Curr. Biol. 31 (18), 4132-4138.e3. https://doi.org/
- Marino, A., Dierking, W., & Wesche, C. (2016). A Depolarization Ratio Anomaly Detector to Identify Icebergs in Sea Ice Using Dual-Polarization SAR Images. IEEE Transactions on Geoscience and Remote Sensing, 54(9), 5602-5615. IEEE Transactions on Geoscience and Remote Sensing. doi: 10.1109/TGRS.2016.2569450.
- Marino, A., Spyrakos, E., González Vilas, L., & Ballester-Berman, J. D. (2019, January 22). Using Sentinel-1 to detect aquaculture structures in Spain.
- Martinez-Porchas, M., Martinez-Cordova, L.R., 2012. World Aquaculture: Environmental Impacts and Troubleshooting Alternatives. Sci. World J. 2012, e389623.
- McInnes, L., Healy, J., & Melville, J. (2020). UMAP: Uniform Manifold Approximation and Projection for Dimension Reduction (arXiv:1802.03426). arXiv. doi: 10.48550/ arXiv.1802.03426.
- Migliaccio, M., Buono, A., Alparone, M., 2022. Microwave satellite remote sensing for a sustainable sea. Europ. J. Remote Sens. 55 (1), 507–519. https://doi.org/10.1080/22797254.2022.2126798.
- Murata, H., Fujii, T., Yonezawa, C., 2023. Evaluating the effect of the incidence angle of ALOS-2 PALSAR-2 on detecting aquaculture facilities for sustainable use of coastal space and resources. PeerJ 11, e14649.
- Ottinger, M., Clauss, K., & Kuenzer, C. (2017). Large-Scale Assessment of Coastal Aquaculture Ponds with Sentinel-1 Time Series Data, Remote Sens., 9(5), Article 5, doi: 10.3390/rs9050440.
- Pedreschi, D., Bouch, P., Moriarty, M., Nixon, E., Knights, A.M., Reid, D.G., 2019. Integrated ecosystem analysis in Irish waters; providing the context for ecosystembased fisheries management. Fish. Res. 209, 218-229. https://doi.org/10.1016/j. fishres 2018 09 023
- Regulation (EU) No 377/2014 of the European Parliament and of the Council of 3 April 2014 Establishing the Copernicus Programme and Repealing Regulation (EU) No 911/2010 Text with EEA Relevance, 122 OJ L (2014). http://data.europa.eu/eli/
- Sahu, P., Chug, A., Singh, A.P., Singh, D., Singh, R.P., 2020. Implementation of CNNs for crop diseases classification: a comparison of pre-trained model and training from scratch. Int. J. Comput. Sci. Netw. Secur. 20 (10), 206–215. https://doi.org/ 10.22937/IJCSNS.2020.20.10.26.
- Shallu, Mehra, R., 2018. Breast cancer histology images classification: Training from scratch or transfer learning? ICT Express 4 (4), 247–254. https://doi.org/10.1016/j. icte, 2018, 10, 007.
- Soldal, I.H., Dierking, W., Korosov, A., Marino, A., 2019. Automatic detection of small icebergs in fast ice using satellite wide-swath SAR images. Remote Sens. (Basel) 11 (7), 806. https://doi.org/10.3390/rs11070806
- Stringham, C., Farquharson, G., Castelletti, D., Quist, E., Riggi, L., Eddy, D., & Soenen, S. (2019). The Capella X-band SAR Constellation for Rapid Imaging. IGARSS 2019 2019 IEEE International Geoscience and Remote Sensing Symposium, 9248-9251. doi: 10.1109/IGARSS.2019.8900410.
- Tajbakhsh, N., Shin, J.Y., Gurudu, S.R., Hurst, R.T., Kendall, C.B., Gotway, M.B., Liang, J., 2016. Convolutional Neural Networks for Medical Image Analysis: Full Training or Fine Tuning? IEEE Trans. Med. Imaging 35 (5), 1299-1312. https://doi. z/10.1109/TMI.2016.2535302
- Tan, J. H. (2024). Pre-training of Lightweight Vision Transformers on Small Datasets with Minimally Scaled Images (arXiv:2402.03752). arXiv. doi: 10.48550/ arXiv.2402.03752.
- Tittensor, D.P., Novaglio, C., Harrison, C.S., Heneghan, R.F., Barrier, N., Bianchi, D., Bopp, L., Bryndum-Buchholz, A., Britten, G.L., Büchner, M., Cheung, W.W.L., Christensen, V., Coll, M., Dunne, J.P., Eddy, T.D., Everett, J.D., Fernandes-Salvador, J.A., Fulton, E.A., Galbraith, E.D., Blanchard, J.L., 2021. Next-generation ensemble projections reveal higher climate risks for marine ecosystems. Nat. Clim. Chang. 11 (11), 973-981. https://doi.org/10.1038/s41558-021-01173-9
- Torres, R., Snoeij, P., Geudtner, D., Bibby, D., Davidson, M., Attema, E., Potin, P., Rommen, B., Floury, N., Brown, M., Traver, I.N., Deghaye, P., Duesmann, B., Rosich, B., Miranda, N., Bruno, C., L'Abbate, M., Croci, R., Pietropaolo, A., Rostan, F., 2012. GMES Sentinel-1 mission. Remote Sens. Environ. 120, 9-24. /doi.org/10.1016/j.rse.2011.05.028
- Ulaby, F. T., Moore, R. K., & Fung, A. K. (1981). Microwave remote sensing: Active and passive. Volume 1. Microwave remote sensing fundamentals and radiometry.

- F.T. Ulaby Ulaby, F. T. (1982). Radar remote sensing and surface scattering and emission
- theory. *Microwave Remote Sensing: Active and Passive*.

 Zou, M., Zhong, Y., 2018. Transfer learning for classification of optical satellite image. Sens. Imag. 19 (1), 6. https://doi.org/10.1007/s11220-018-0191-1.
- Zuhlke, M., Fomferra, N., Brockmann, C., Peters, M., Veci, L., Malik, J., & Regner, P. (2015). SNAP (Sentinel Application Platform) and the ESA Sentinel 3 Toolbox. 734, 21. Sentinel-3 for Science Workshop.